ELSEVIER

Materials Chemistry and Physics 61 (1999) 244–250

MATERIALS CHEMISTRY AND PHYSICS

www.elsevier.com/locate/matchemphys

Structure-related optical properties of rapid thermally annealed $Ba_{0.7}Sr_{0.3}TiO_3$ thin films

Yu-Fu Kuo, Tseung-Yuen Tseng*

Department of Electronic Engineering and Institute of Electronics, National Chaio-Tung University, Hsinchu 30050, Taiwan

Received 9 March 1999; received in revised form 17 June 1999; accepted 23 June 1999

Abstract

Polycrystalline thin films of $Ba_{0.7}Sr_{0.3}TiO_3$ (BST) are deposited on SiO_2/Si substrates by radio frequency magnetron sputtering. This work also examines how the O_2 atmosphere annealing temperature affects not only the crystalline and morphological properties, but also the refractive index and the optical band gap energy. The BST films possess the highest dense packing growth and near-bulk optical properties as the O_2 atmosphere annealing temperature increases. Analysis results indicate that the packing density and the refractive index of BST films increase as the annealing temperature increases, whereas the optical band gap energies apparently decreased. In addition, the dispersion of the refractive index is analyzed in terms of dispersion parameters using the single oscillator dispersion model of Wemple and DiDomentico.

Keywords: BST; Thin film; Annealing; Optical properties

1. Introduction

Ferroelectric thin films of high dielectric material such as $(Ba_{1-x}Sr_x)TiO_3$ have been widely investigated for their feasibility in thin film integrated capacitors and storage capacitors in gigabit dynamic random access memory (DRAM) applications [1]. The large electro-optical coefficient of this material is also highly promising for optical applications [2]. In addition, the thin films or multilayer systems of BST can be used in nonlinear optical devices such as planar waveguides or optical switches with minimal optical propagation losses. Most optical losses are directly related to the thin film growth process and the film structure that develops [3,4].

Some investigations have focused on the dependence of optical properties and film structure on the deposition parameters of thin films deposited by various methods such as sputtering [5], sol–gel process [6], and pulsed laser deposition [7–10]. The published data on refractive indices and dispersion parameters, as well as on fundamental optical band gap energies, suggest that the optical properties and the crystalline and morphological structures of these perovskite thin film materials are strongly interdependent.

For $(Ba_{1-x}Sr_x)TiO_3$ thin films, no detailed studies have elucidated the optical and optoelectronic properties related to the thin film growth process in radio-frequency (RF) magnetron sputtering. Therefore, this work investigates the optical properties of $Ba_{0.7}Sr_{0.3}TiO_3$ (BST) thin film as a function of various oxygen ambient annealing temperature after RF magnetron sputtering deposited. The real and imaginary parts of the complex index of refraction, $n(\lambda)$ (refraction index) and $k(\lambda)$ (extinction coefficient), were obtained from a Nikon n&k Analyzer 1200. Next, the optical dispersion parameters were determined and explained on the basis of the Wemple single electronic oscillator dispersion model which is frequently used to correlate linear optical dispersion data with the fundamental band gap of thin film materials.

2. Experimental procedure

A ceramic target used to prepare BST thin films on SiO_2(100 nm)/Si substrates by RF magnetron sputtering deposition, having a diameter of 2 in. and a thickness of 1/4 in., was prepared from $BaCO_3$, $SrCO_3$ and TiO_2 powders (purity 99.99%) using standard solid state reaction process. All BST films were prepared at a fixed power of 100 W (power density of 4.93 W/cm^2) and a constant pressure of

*Corresponding author.
E-mail address: tseng@cc.nctu.edu.tw (T.-Y. Tseng)

0254-0584/99/$ – see front matter
PII: S0254-0584(99)00157-1

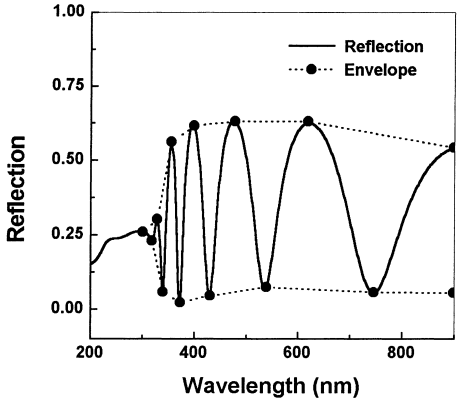

Fig. 1. Reflection pattern of a 750°C annealing $Ba_{0.7}Sr_{0.3}TiO_3$ film with reflection envelopes.

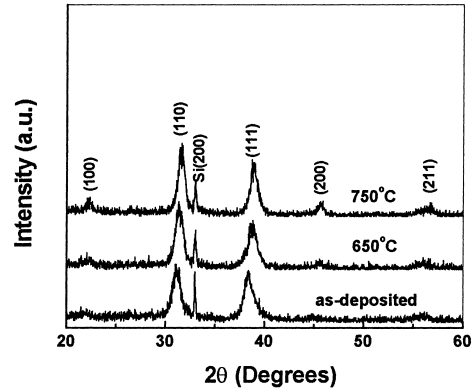

Fig. 2. XRD patterns of $Ba_{0.7}Sr_{0.3}TiO_3$ films annealed at various temperatures.

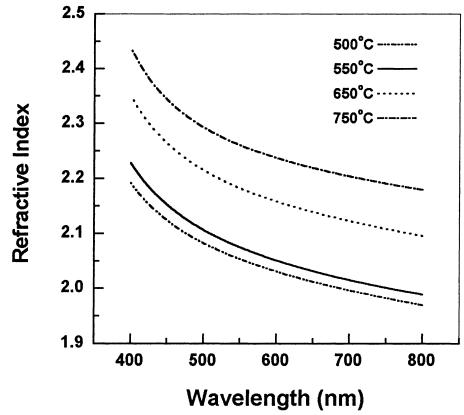

Fig. 3. Variation of refractive index with wavelength for various annealing temperatures films.

30 mTorr while maintaining an argon to oxygen ratio of 8 : 2. The constant substrate temperature of 500°C W as used. The film thickness was about 415 nm. The deposited rate was about 3.4 nm/min. After deposition, the films were heat treated with the rapid thermal anneal (RTA) in O_2 ambient at various temperatures from 500 to 750°C for 30 min.

The crystallinity of the films was characterized by X-ray diffraction (XRD, MAC science M18, Japan). To determine the optical constants $n(\lambda)$ and $k(\lambda)$ and the thickness of the BST films, optical reflection spectra were measured in the wavelength range 180–900 nm with Nikon n&k Analyzer 1200. Fig. 1 illustrates a typical reflection pattern of BST film, together with the envelopes of the reflection extrema of the front surface reflection. The reflection spectral data were analyzed and fitted using the BST model built-in Nikon n&k Analyzer 1200. The film thickness can be determined from the wavelength position and the interference order of the reflection minima and maxima indicated in Fig. 1. Scanning electron microscopy (SEM, HITACHI Model S-4000, Japan) was also used to measure the film thickness which was compared with the thickness calculated from the reflection spectrum.

3. Results and discussion

3.1. Structure

Fig. 2 displays the XRD patterns of films as a function of annealing temperature in O_2 atmosphere. As the annealing temperature increased, the peaks in the XRD patterns became more intense and the full-width at half maximum (FWHM) decreased. The average grain size of the films can be estimated from the FWHM using Scherrer's equation [11,12]. The results indicated better crystallinity and an increase in grain size (from 8.8 to 10.8 nm) with an increasing annealing temperature.

The XRD patterns in Fig. 2 reveal a gradual shift of 2θ angles to the high angle side, indicating the shrinkage of perovskite lattice by increasing the annealing temperature. The lattice constants of the BST films determined from the XRD patterns monotonously decrease from $a = 4.038$ Å in as-deposited film to $a = 3.987$ Å in 750°C annealing film, the films have a larger lattice constant than that of bulk material. This phenomenon is also frequently observed in sputtered $BaTiO_3$ base thin films, indicating non-equilibrium and highly distorted states within the films [13,14].

3.2. Optical and optoelectronic properties

Fig. 3 depicts the dispersion of the refractive index spectra as a function of wavelength for BST films annealed at various temperatures in O_2 atmosphere for 30 min. According to Fig. 3, the dispersion curve rises sharply toward shorter wavelengths, displaying the typical shape of a dispersion curve near an electronic interband transition. The strong increase in the refractive index is associated with the fundamental band gap absorption. Fig. 4 presents the measured refractive indices of the films with various annealing temperatures. As for films annealed at high temperatures, the refractive indices are higher than as-deposited film and increased from 0.25% (500°C) to 10.7% (750°C). This

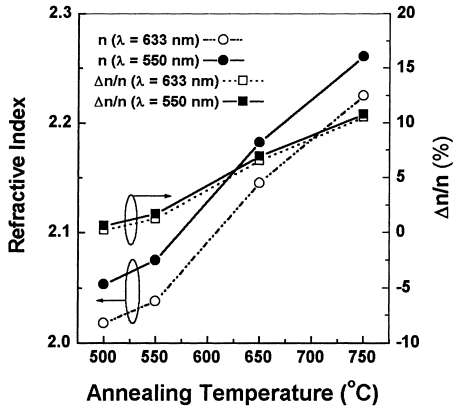

Fig. 4. Refractive indices n_f of $Ba_{0.7}Sr_{0.3}TiO_3$ films annealed at various temperatures.

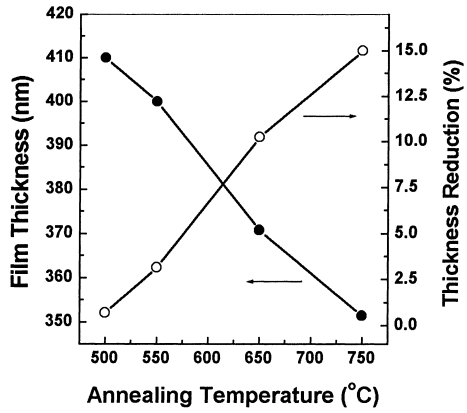

Fig. 5. Thickness of $Ba_{0.7}Sr_{0.3}TiO_3$ films annealed at various temperatures.

difference may be owing to that annealing under O_2 atmosphere at an elevated temperature increases film's crystallinity and packing density. According to Fig. 5, the thickness of as-deposited films reduced after annealing at various temperatures in O_2 ambient. The thickness reduced from 0.7% (500°C) to 15% (750°C), possibly resulting in increased packing density for the film with an elevated annealing temperature. The similar phenomenon has been found in other studies [15]. The film thickness values were also verified by SEM observation and were found to agree within 10 nm.

Notably, the packing densities of the film and the bulk material can be calculated from the refractive index data. The packing density (p) is defined as the ratio of the average film density (ρ_f) and the bulk density (ρ_b):

$$p = \frac{\rho_f}{\rho_b} \tag{1}$$

The correlation between the packing density and the refractive index can be expressed as [16,17]:

$$p = \frac{\rho_f}{\rho_b} = \frac{n_f^2 - 1}{n_f^2 + 2} \times \frac{n_b^2 + 2}{n_b^2 - 1} \tag{2}$$

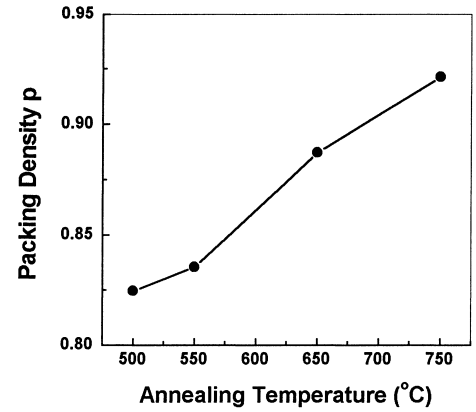

Fig. 6. Packing density of $Ba_{0.7}Sr_{0.3}TiO_3$ films annealed at various temperatures.

where n_f denotes the refractive index of the film, n_b the refractive index of the bulk. By assuming that the bulk value of the refractive index of BST is 2.465 at $\lambda = 550$ nm [8], the packing density in various annealing temperatures is shown in Fig. 6. Fig. 7 illustrates the refractive index ($\lambda = 550$ nm) versus the packing density for BST films on the basis of the results of Figs. 4 and 6. According to Fig. 7, a small packing density reduces the film's refractive index. The packing density has a markedly increased value (from 0.82 to 0.92) due to a higher annealing temperature. A higher annealing temperature not only increases the mobility of atoms or molecules of the film, but also enhances the formation of large and more closely packed crystals. Hence, an increase in grain size (from 8.8 to 10.8 nm) and a decrease in grain boundary area and voids occur.

Thin oxide films deposited by RF magnetron sputtering generally have a columnar structure with pores at high deposition temperature [8,18,19]. Some of these pores are empty or filled with water. Therefore, the relative film density (packing density) is lower than that of the bulk material. In order to understand the growth morphology and relation between the refractive index of the film n_f and that of the bulk n_b which contain a certain volume part of voids,

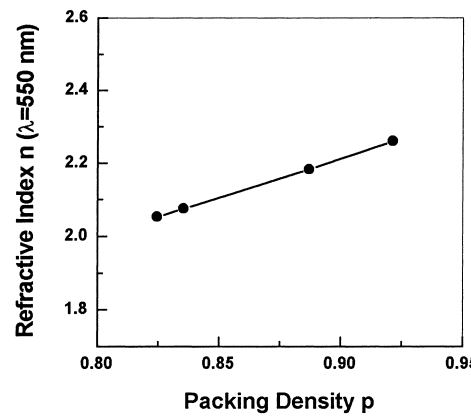

Fig. 7. Refractive index n ($\lambda = 550$ nm) versus the packing density p of BST thin films.

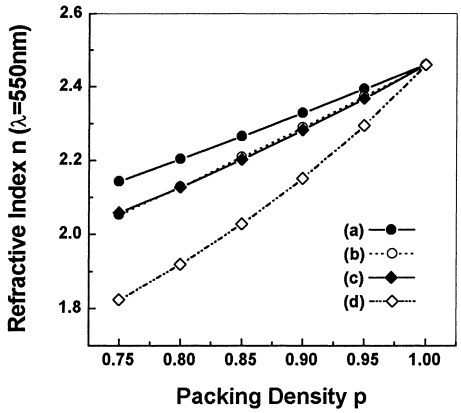

Fig. 8. Refractive index n ($\lambda = 550$ nm) versus the packing density p for two microstructures calculated according to the Bragg–Pippard model: (a) close-packed columns with filled voids; (b) close-packed columns with empty voids; (c) columnar growth with filled voids; (d) columnar growth with empty voids.

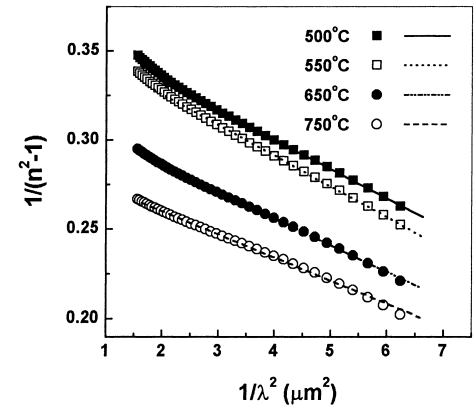

Fig. 9. The single electronic oscillator model fitting of $Ba_{0.7}Sr_{0.3}TiO_3$ films with various annealing temperatures.

the effective medium mode of Bragg and Pippard can be used on the basis of the growth morphology of the film [20–22]. A close-packed columnar grain morphology is given by

$$n_f^2 = \frac{n_b^2 p + (2-p)n_b^2 n_p^2}{(2-p)n_b^2 + p n_p^2} \tag{3}$$

and a columnar structure of reduced density is given by

$$n_f^2 = \frac{(1-p)n_p^4 + (1+p)n_p^2 n_b^2}{(1+p)n_p^2 + (1-p)n_b^2} \tag{4}$$

where n_p denotes the refractive index of the voids, which may be 1 for empty voids or 1.33 in the case of water-filled voids [23–25].

Fig. 8 depicts the dependence of the refractive index n_f ($\lambda = 550$ nm) of two microstructures calculated according to the Bragg–Pippard mode with empty and water-filled voids. Comparing Fig. 8 with Fig. 7, it reveals that a good fitting in packing density can be achieved from 0.75 to 0.9 by the mode of close-packed columns with empty voids (line (b) in Fig. 8) and columnar growth with water-filled voids (line (c) in Fig. 8). In order to distinguish these two modes, the dependence of the dispersion parameters E_o and E_d on the O_2 ambient annealing temperature must be determined.

The dispersion data of the refractive index can be interpreted in terms of the individual dipole oscillator mode [26,27], i.e. assuming that the medium contains elastically bound particles capable of vibrating with the same natural frequency of oscillation ν_o. The refractive index as a function of wavelength, $n(\lambda)$, can be expressed as :

$$n(\lambda)^2 - 1 = \frac{E_o E_d}{E_o^2 - (hc/\lambda)^2} \tag{5}$$

where c denotes the light speed, h Plank constant, E_o the single-oscillator energy and E_d the dispersion energy. The dispersion data of the refractive index also can be analyzed by using Sellmeir dispersion formula that is given by:

$$n(\lambda)^2 - 1 = \frac{S_o \lambda_o^2}{1-(\lambda_o/\lambda)^2} \tag{6}$$

where S_o is an average oscillator strength and λ_o is an average oscillator wavelength. Fig. 9 displays the optical dispersion behavior of BST thin films annealed at various temperatures in O_2 atmosphere, $(n^2-1)^{-1}$ versus λ^{-2} plot, where E_d, E_o, S_o and λ_o are deduced from the slope of the resulting straight fitting line and from the infinite wavelength intercept, respectively.

The study also determined the dependence of the dispersion parameters E_o and E_d on the annealing temperature. Fig. 10(a) and (b) depict the calculated dependence of the Wemple dispersion parameters E_o and E_d for different O_2 atmosphere annealing temperatures and packing densities. According to our results, E_o depended only slightly on the annealing temperature, with a small decrease to about 5.93 eV. On the other hand, the annealing temperature significantly affects the dispersion energy E_d in a manner qualitatively similar to the refractive index n. According to these figures, the dispersion energy E_d increases rapidly with an increasing annealing temperature. The values of E_d and E_o for the film annealing at 750°C are 22 and 5.85 eV, respectively, which agrees well with the reported bulk values for $BaTiO_3$ ($E_d = 24.0$ eV, $E_o = 5.63$ eV) [26,27] and $SrTiO_3$ ($E_d = 23.7$ eV, $E_o = 5.68$ eV) [26,27] and thin film value for $Ba_{0.65}Sr_{0.35}TiO_3$ [8]. This manner appears to be qualitatively similar to the reported result of changes in the dispersion coefficients E_d and E_o with the relative packing density. A higher annealing temperature increases the packing density, which correlates with the situation in Fig. 6. The increase in dispersion energy E_d at a higher annealing temperature may be attributed to the increased packing density. The only slightly dependence of E_o in O_2 atmosphere annealing temperature and packing density suggests that the films are most likely composed with empty voids [8].

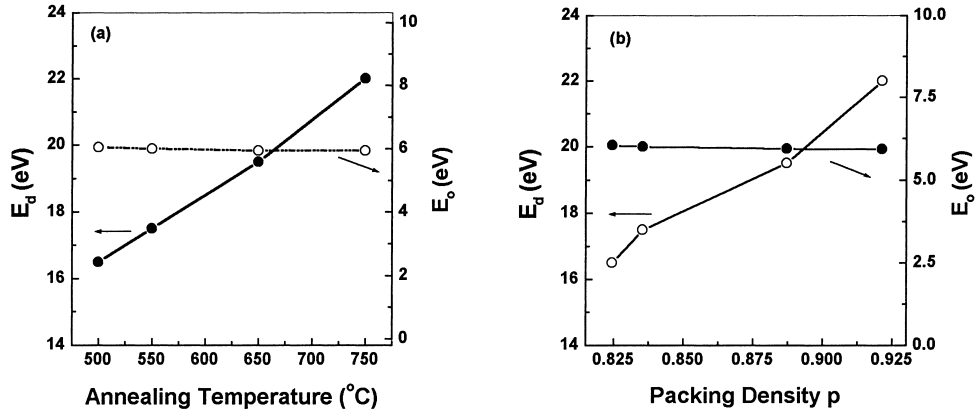

Fig. 10. Changes in the dispersion coefficients E_d and E_o with (a) various annealing temperatures; (b) the relative packing density.

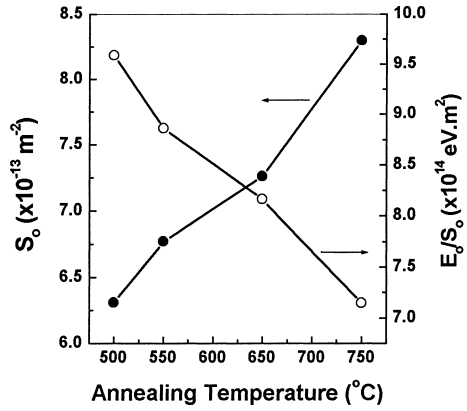

Fig. 11. The average oscillator strength and the energy dispersive parameter E_o/S_o of $Ba_{0.7}Sr_{0.3}TiO_3$ films with various annealing temperatures.

Fig. 11 depicts the average oscillator strength S_o and the ratio of E_o/S_o as a function of annealing temperature. According to Fig. 11, S_o increases with an increasing the annealing temperature while, at the same time, E_o/S_o decreases. The values of S_o, λ_o and E_o/S_o were estimated to 8.3×10^{13} m^{-2}, 209 nm (Fig. 12) and 7.3×10^{-14} eV/m^2, respectively, for the film annealing at 750°C, which closely corresponds to the reported bulk values for $BaTiO_3$ ($S_o = 9.1, 8.4 \times 10^{13}$ m^{-2}, $E_o/S_o = 6.4, 6.6, 7.4 \times 10^{-14}$ eV/m^2) [9,27,28] and $SrTiO_3$ ($S_o = 8.9 \times 10^{13}$ m^{-2}, $E_o/S_o = 6.5, 7.4 \times 10^{-14}$ eV/m^2) [9,26,28].

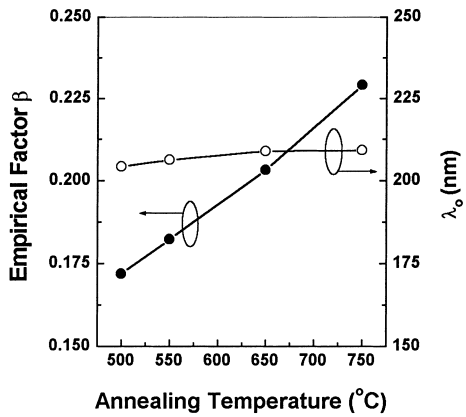

Fig. 12. The empirical factor and the average oscillator wavelength of $Ba_{0.7}Sr_{0.3}TiO_3$ films with various annealing temperatures.

The dispersion energy can be correlated with the coordination with the nearest neighbors and the effective electronic charge as recommended in [27] by

$$\beta = \frac{E_d}{N_c} Z_e N_e \tag{7}$$

where N_c denotes the coordination number of the cations to their nearest-neighbor anions, Z_e the valence number of the anions, N_e the number of valence electrons, and β an empirical factor which is given as 0.26 ± 0.04 eV for most oxides containing a single anion [26,27]. Fig. 12 indicates that the calculated value of β increases with an increasing annealing temperature. The observed β of the film annealing at 750°C is 0.23 which is close to the bulk $BaTiO_3$ ($\beta = 0.24$, 0.25) and bulk $SrTiO_3$ ($\beta = 0.25$) and correlates well with many other bulk oxides [26,27].

The optical band gap energy E_{gap} of each film was deduced from the spectral dependence of the absorption constant $\alpha(\lambda)$ by applying the Tauc relation [29]:

$$\alpha(\lambda)E \approx A(E - E_{gap})^{1/r} \tag{8}$$

where A is a constant, and $r = 1/2$, 2, 3/2 or 3 for allowed direct, allowed indirect, forbidden direct and forbidden indirect electronic transitions, respectively [30,31]. The absorption constant $\alpha(\lambda)$ was determined from each reflection spectrum using a reflection extrema envelope method described in detail elsewhere [32,33]. Once $\kappa(\lambda)$ is obtained from the n&k analyzer 1200, $\alpha(\lambda)$ can be calculated from the equation:

$$\kappa(\lambda) = \frac{\alpha(\lambda)\lambda}{4\pi} \tag{9}$$

The $(\alpha E)^{1/r}$ versus E plots were found to give a linear dependence with $r = 1/2$, as shown in Fig. 13, corresponding to a direct allowed transition. In the higher energy region of

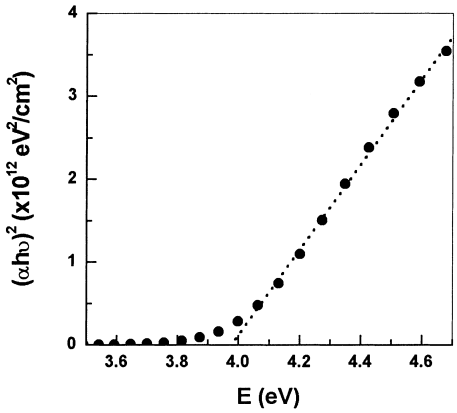

Fig. 13. Plot of $(\alpha h\nu)^2$ vs. photon energy $h\nu$ for a 750°C annealing film. The optical band gap energy is deduced from the extrapolation of the straight line to $(\alpha h\nu)^2 = 0$.

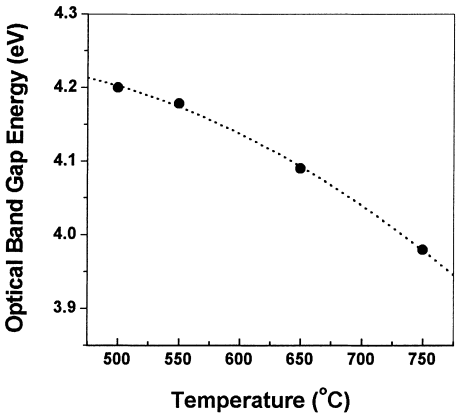

Fig. 14. Optical band gap energies of $Ba_{0.7}Sr_{0.3}TiO_3$ films annealed at various temperatures.

the absorption edge, $(\alpha E)^2$ varied linearly with E. In the low energy region of the edge, the absorption spectrum deviated from the straight line plot. Notably, the straight line behavior of $(\alpha E)^2$ versus. E plot in the high energy range was taken as the prime evidence for a direct allowed electronic transition between the highest occupied state of the valence band and the lowest unoccupied state of the conduction band. The optical band gap was determined by extrapolating the linear portion of the plot to $(\alpha E)^2 = 0$. Fig. 14 illustrates the optical band gap energies (E_{gap}) for films of different annealing temperatures. The E_{gap} decreases from 4.2 to 3.98 with the increasing annealing temperature up to 750°C. Kumar and Mansingh [34] suggested that the decrease in the optical band gap energy value in annealing might be attributed to the lowering of the interatomic spacing, which reduced the polarization and electron–hole interaction corrections. The ratios between the optical band gap energies E_{gap} and the experimental Wemple oscillator energies E_o of the films were determined to be relatively constant factors of 1.47–1.5, which correlates well with most oxides ($E_o \approx 1.5E_{gap}$) [26,27]. However, the different values have been reported for BST films with different crystalline structures and composition deposited by various deposition techniques [5,8–10]. Recent investigations involving the dependence of the optical band gap energies of polycrystalline sputtered $BaTiO_3$ films on the grain size suggest a size effect of the optical band gap energy [35]. Those investigations also demonstrated that the optical band gap energies decrease with an increasing grain size. Thielsch et al. [8] and Panda et al. [5] also observed that the optical band gap energy increases with an increasing strontium concentration in the film. In this work, the optical band gap energy decreased from about 4.20 eV for a mean grain size of 8.8 nm, to 3.98 eV for a grain size of about 10.8 nm which is higher than E_{gap} of polycrystalline sputtered $BaTiO_3$ films [35] with 3.68 eV for a mean grain size of 8 nm, to 3.53 eV for a grain size of about 35 nm.

4. Conclusion

Thin films of $Ba_{0.7}Sr_{0.3}TiO_3$ (BST) were prepared on the SiO_2/Si substrates with radio frequency magnetron sputtering. This work also examined how the O_2 atmosphere annealing temperature affects the crystalline structure, the grain growth and the optical and optoelectronic properties. According to our results, the packing density, the grain size and the refractive index of the films increased with an increasing annealing temperature. The films exhibit the highest dense packing growth and near-bulk optical properties as the O_2 atmosphere annealing temperature increases. The optical band gap energy depends on the grain size and, becomes smaller for films with a larger grain size. The dispersion of the refractive index was also analyzed in terms of the parameters E_o and E_d using the single oscillator dispersion model of Wemple and DiDomentico. Our experimental results about Wemple oscillator energies E_o ($\approx 1.49E_{gap}$) and the empirical factor $\beta \approx 0.23$ of the 750°C annealing films closely correspond with most reported data ($E_o \approx 1.5E_{gap}$ and $\beta \approx (0.26 \pm 0.04)$ eV).

References

[1] K. Kim, C.G. Hwang, J.G. Lee, IEEE Tran. Elec. Dev. 45 (1998) 598.
[2] B. Biharj, J. Kumar, G.T. Stauf, P.C. Van Buskirk, C.S. Hwang, J. Appl. Phys. 76 (1994) 1169.
[3] K.H. Gunther, Appl. Opt. 23 (1984) 3612.
[4] C.G. Granqvist, O. Hunderi, Phys. Rev. B 16 (1977) 3513.
[5] B. Panda, A. Dhar, G.D. Nigam, D. Bhattacharya, S.K. Ray, Thin Solid Films 332 (1998) 46.
[6] I. Suzuki, M. Ejima, K. Watanbe, Y.M. Xiong, T. Saitoh, Thin Soild Films 313–314 (1998) 214.
[7] A.C. Carter, W. Chang, S.W. Kiechoefer, J.S. Horwitz, D.B. Chrisey, Appl. Phys. Lett. 71 (1997) 3353.
[8] R. Thielsch, K. Kaemmer, B. Holzapfel, L. Schultz, Thin Solid Films 301 (1997) 203.
[9] F. Tcheliebou, H.S. Ryu, C.K. Hong, W.S. Park, S. Baik, Thin Solid Films 305 (1997) 30.

[10] H.F. Cheng, J. Appl. Phys. 79 (1996) 7965.
[11] A.J.C. Wilson, X-ray Optics, Methuen, London, 1949, p. 45.
[12] W.A. Ranchinger, J. Sci. Instrum. 25 (1984) 254.
[13] Y.F. Kuo, T.Y. Tseng, Electrochemical and Solid-State Lett. 25 (1999) 236.
[14] T.S. Kim, C.H. Kim, M.H. Oh, J. Appl. Phys. 75 (1994) 7998.
[15] M.H. Suhail, G.M. Rao, S. Mohan, J. Appl. Phys. 71 (1992) 1421.
[16] G. Bauer, Ann. Phys. 19 (1934) 434.
[17] R. Jacobson, Phys. Thin Films 8 (1975) 51.
[18] B.A. Movchan, A.V. Demshishin, Fizika Metal 28 (1969) 653.
[19] J.A. Thornton, J. Vac. Sci. Technol. 11 (1974) 666.
[20] W.L. Bragg, A.B. Pippard, Acta Crystallogr. 6 (1953) 865.
[21] H.A. Mcleod, J. Vac. Sci. Technol. A 4 (1986) 418.
[22] R. Thielsch, Proc. 2nd Conf. On Future Applications of Thin Films in Micro-, Opto-, and Bio-electronics, and Optics, TU Karl-Marx-Stadt Conf. Proc., vol. 6, 1989, p. 160.
[23] H.K. Pulker, Appl. Opt. 18 (1979) 1969.
[24] G.M. Hale, M.R. Querry, Appl. Opt. 12 (1973) 555.
[25] H. Koch, Phys. Stat. Solidi 12 (1965) 533.
[26] M. Didomenico Jr., S.H. Wemple, J. Appl. Phys. 40 (1969) 720.
[27] S.H. Wemple, M. Didomenico Jr., Phys. Rev. B 3 (1971) 1338.
[28] A. Mansingh, C.V.R. Vasanta Kumar, J. Mat. Sci. Lett. 7 (1988) 1104.
[29] J.C. Tauc, Optical Properties of Solids, North-Holland, Amsterdam, 1972, p. 372.
[30] N.F. Mott, E.A. Davis, Electronic Processes in Non-crystalline Materials, 2nd ed., Clarendon Press, Oxford, 1979.
[31] J. Tauc, A. Menth, J. Non-Cryst. Solids 8–10, (1972) 569.
[32] D.B. Kushev, N.N. Zheleva, Y. Demokopoulou, D. Siapkas, Infrared Phys. 26 (1986) 385.
[33] N.F. Minkov, J. Phys. D: Appl. Phys. 22 (1989) 1157.
[34] C.V.R. Vasant Kumar, A. Mansingh, 7th IEEE Int. Symp. on Application of Ferroelectrics, IEEE Press, New York, 1990, p. 713.
[35] X.M. Lu, J.S. Zhu, W.Y. Zhang, G.Q. Ma, Y.N. Wang, Thin Solid Films 274 (1996) 165.